Velocity spectra and angular distributions of evaporation residues from $^{32}S + ^{12}C$ at 145 MeV

N. Arena, Seb. Cavallaro, S. Femino', P. Figuera, S. Pirrone, F. Porto, and S. Sambataro
Dipartimento di Fisica, Universitá di Catania, Universitá di Messina, Istituto Nazionale di Fisica Nucleare, Sezione di Catania and Laboratorio Nazionale del Sud I-95129 Catania, Italy
(Received 25 April 1991)

Velocity spectra and angular and mass distributions for the evaporation residues of the $^{32}S+^{12}C$ system at $E_{^{32}S}=145$ MeV in the angular range $3° \leq \vartheta_L \leq 12°$ have been measured. In order to separate compound nucleus evaporation residues from other heavy reaction products, a kinematic analysis based on simple statistical assumptions relative to the velocity spectra was performed. The structures in the mass distribution are compared with the LILITA code predictions. The fusion excitation function of the existing results is compared with theoretical models. The total reaction cross section has been extracted by means of the modified sum of differences method.

I. INTRODUCTION

The fusion cross sections for the system $^{32}S+^{12}C$, reported in previous works, have been measured at bombarding energy not far above the Coulomb barrier (region I) [1] and at higher energy (region II) [2,3]. In these last two works it was assumed that the evaporation residue cross section of the reaction products with $Z > 16$ may be identified with the fusion cross section. This is somewhat arbitrary but it may be justified by the general assumption that the formation and decay of an equilibrated compound nucleus is the main reaction mechanism in the heavy-ion collision at low energies. At these energies, the projectile fuses with the target and the decay of the compound nucleus proceeds via the emission of light particles resulting in the evaporation residue's formation. At higher incident energies, this picture begins to be more and more invalid. When the incident energy increases, exceeding about 10 MeV/nucleon for normal kinematics (i.e., a light projectile on a heavier target), only a part of the projectile fuses with the target nucleus, while the remaining part continues nearly undeflected with approximately the beam velocity. For the so-called "inverse kinematics," part of the target fuses with the whole projectile. These processes are called incomplete fusion [4–6]. Recent investigations on incomplete fusion suggest a dependence of this process on the degree of mass asymmetry in the entrance channel [7–10]. However, several observations moderate the above general statement. The exact nature of the onset of incomplete fusion and the energy at which it occurs is still controversial, at least for light systems. For some authors [7,11,12], there is an evidence of a threshold velocity for the onset of the incomplete fusion process, while other authors, in recent studies [13] on the reactions induced by ^{12}C at 5.5–10 MeV/nucleon, observe incomplete fusion components in the full energy range. These last authors suggest that the incomplete fusion should be viewed as a process which is always in competition with the complete fusion one, although its relative importance grows with the energy.

In this paper, we present the measurements of the fusion and elastic cross sections for the $^{32}S+^{12}C$ system at $E_{^{32}S}=145$ MeV, and we report the total reaction cross section as obtained from them. The present work was performed both to reduce the lack of experimental data in the second energy region and to explore the possible existence of an incomplete fusion component in the evaporation residue cross section also at this low energy. For these reasons we detected and identified the evaporation residues with a time-of-flight (TOF) technique in a wide angular range and we analyzed the velocity spectra and the angular distributions.

The experimental procedures are described in the next section while the analysis of experimental results is explained in Sec. III. In Sec. IV the results of this analysis are discussed and compared to the predictions of theoretical models. Finally, the conclusions are presented in the last section.

II. EXPERIMENTAL PROCEDURE

The experiment was performed at the SPM Tandem accelerator facility of the Laboratorio Nazionale del Sud (LNS) in Catania. Beams of ^{32}S ions at an energy of 145 MeV were incident on a ^{12}C target of 40 $\mu g/cm^2$ nominal thickness, placed perpendicular to the beam direction. The oxygen and the nitrogen content in the target were found to be negligibly small.

Heavy reaction products ($Z \geq 16$, $A \geq 32$) were identified by means of the experimental apparatus, described in detail in Refs. [14–16] and schematically sketched in Fig. 1. The setup consists of a sliding seal scattering chamber, 45 cm in diameter, which can be rotated around the target axis, and is rigidly connected to a gas detector system by means of a 118-cm flight path. The gas detector system consists of two volumes: the big one is just the ionization chamber, while the small one houses a parallel plate avalanche counter (PPAC). A 20-cm^2 surface window, made of a thin layer of polipropylene supported by a grid, separates the small volume from the high vacuum. A second window is placed between the PPAC and the ionization chamber because the

 ©1991 The American Physical Society

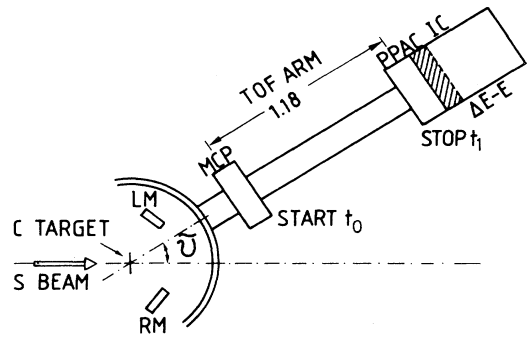

SIGNAL	DETECTOR	RESOLUTION (145 MeV)
ΔE	IONIZATION CHAMBER	1 MeV FWHM (3.0%)
E	IONIZATION CHAMBER	1.1 MeV FWHM (0.8%)
TOF = $t_1 - t_0$	MCP-PPAC	300 ps FWHM (1.0%)

ΔΩ = 1 msr

FIG. 1. The experimental apparatus and resolution performances for the 145-MeV $^{32}S+^{12}C$ reaction.

two detectors cannot operate in the same gas volume. To reduce the straggling, the windows were made of polipropylene foils thinned to about 30 μg/cm.^{2} This thickness was largely sufficient to hold the pressure of about 100 Torr, required to stop 145-MeV ^{32}S ions in the ionization chamber.

The particles were stopped in the P10 gas mixture filling the ionization chamber whose anode was divided in two sections, a ΔE plate 10 cm long and a E_R plate 65 cm long, in order to obtain the Z identification of the detected particles. A typical example of the Z resolution is shown in Fig. 2.

The mass identification was obtained by using the energy $E = E_R + \Delta E$ deposited in the ionization chamber and the time of flight as measured by a microchannel plate (MCP) placed behind the exit of the scattering chamber and by a PPAC placed in front of the ionization chamber. The PPAC, having a 20-cm^2 surface and a 3-mm gap, operated with a steady flow of isobutane at 3 Torr. An overall time resolution, lower than 300 ps FWHM, was obtainable without extreme carefulness, while the energy resolution of the ionization chamber was approximately 0.6% at the elastic-scattering energy. The mass resolution so obtained allowed a careful separation for all the evaporation residues. Figure 3 shows the mass spectra for each $Z > 16$ detected at $\vartheta_L = 10°$.

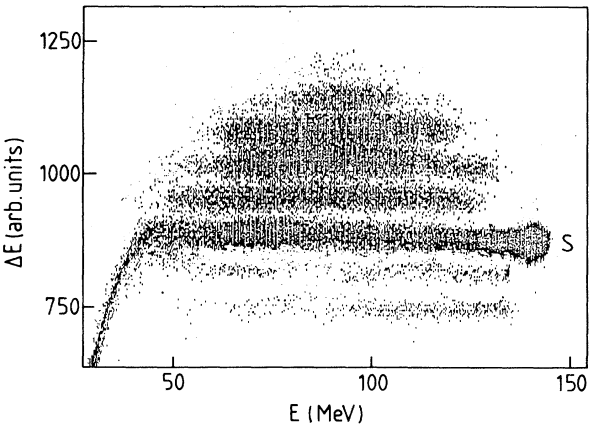

FIG. 2. Scatter plot of ΔE vs energy for the reaction $^{32}S+^{12}C$ at the bombarding energy 145 MeV and a laboratory angle of 6°.

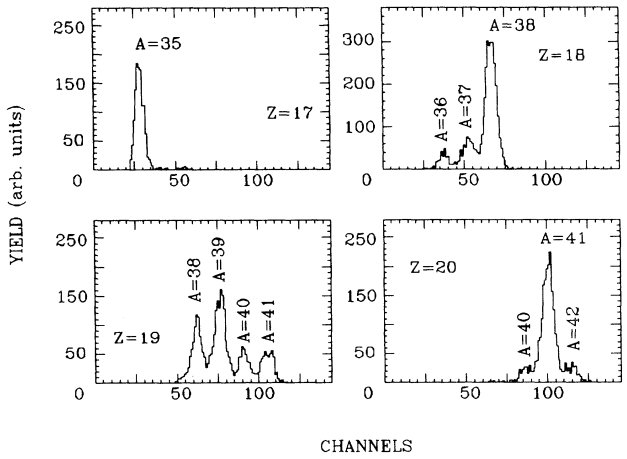

FIG. 3. Mass spectra of the evaporation residues for each $Z > 16$ detected at $\vartheta_L = 10°$.

Two silicon surface-barrier detectors, placed at ±7° with respect to the beam axis, were used to monitor the $^{32}S+^{12}C$ elastic-scattering yield during the experiment in order to obtain the relative normalization of the measured differential cross section. The absolute normalization was obtained by comparing the elastic-scattering data to the Rutherford scattering cross section at very forward angles.

III. EXPERIMENTAL RESULTS AND ANALYSIS

A. Elastic-scattering and total reaction cross section

The elastic-scattering angular distribution was measured in the angular range $3° \leq \vartheta_L \leq 12°$ in steps of 0.5° at forward angles and 1.0° at larger angles. In Fig. 4 the experimental ratios $\sigma_{el}(\vartheta)/\sigma_R(\vartheta)$ between the elastic and Rutherford cross sections versus the center-of-mass angle are reported. The solid line in the same-figure corresponds to an optical model fit obtained by using PTOLEMY code [17] with the parameters of Table I.

In order to determine the total reaction cross section σ_r we used the modified sum of differences (MSOD) method, which has been shown to be a useful tool for extracting σ_r from the experimental elastic-scattering data [18,19]. We recall that the practical procedure for evaluating σ_r consists of constructing the functions

TABLE I. Elastic-scattering optical model fit parameters. Only the well depths V_R and V_I were allowed to vary during the fit.

V_R (MeV)	V_I (MeV)	r_{OR} (fm)	r_{OI} (fm)	a_R (fm)	a_I (fm)
20.5	32.6	1.3	1.19	0.55	0.55

$I(\vartheta)=2\pi[\sigma_R(\vartheta)-\sigma_{el}(\vartheta)]\sin\vartheta$ and $\sigma_r(\vartheta)=\int_\vartheta^\pi I(\vartheta)d\vartheta$, where $\sigma_R(\vartheta)$ and $\sigma_{el}(\vartheta)$ are the Rutherford and elastic-scattering cross sections in the center-of-mass system, respectively. As suggested in Refs. [18,19] the ϑ_0 angle at which the function $I(\vartheta)$ attains its last minimum is chosen as starting angle in order to determine the σ_r value, so that $\sigma_r=2\pi\int_{\vartheta_0}^\pi[\sigma_R(\vartheta)-\sigma_{el}(\vartheta)]\sin\vartheta\, d\vartheta$.

In Fig. 5, we report the integrand function $I(\vartheta)$ and the values of the function $\sigma_r(\vartheta)$ versus ϑ. The value of the total reaction cross section so extracted is 1446±60 mb, which is in excellent accord with the value of 1460 mb as obtained by means of the optical model analysis.

B. Velocity spectra

The velocity spectra of the reaction products were obtained from the MCP-PPAC time measurements. In Figs. 6 and 7 typical velocity distributions for reaction products, covering the mass range $A=35$–41, are shown for $\vartheta_L=3°$ and 5°, respectively. The experimentally measured differential cross section $d^2\sigma/d\Omega_L dV_R$ divided by V_R^2 has been fitted with the evaporation residue velocity distribution, theoretically obtained with the simple assumption [20] that the angular distributions for all the emitted light particles are isotropic in the mass center system. According to this assumption, the velocity distributions of the heavy residues has the symmetric Gaussian form

$$\frac{1}{V_R^2}\frac{d^2\sigma}{d\Omega_L dV_R}=k\exp\left[-\frac{V_{CN}^2\sin^2\vartheta_L}{2s^2}\right]\times\exp\left[-\frac{(V_R-V_{CN}\cos\vartheta_L)^2}{2s^2}\right]. \quad (1)$$

Here $V_{CN}\cos\vartheta_L$ is the Gaussian centroid, s is the FWHM width, V_R and ϑ_L are respectively the laboratory velocity and the angle at which the heavy residue is detected, and k is a normalization constant. The results of the fitting are shown in Figs. 6 and 7 as continuous curves. The simple Gaussian distribution predicted in Eq. (1) is clear-

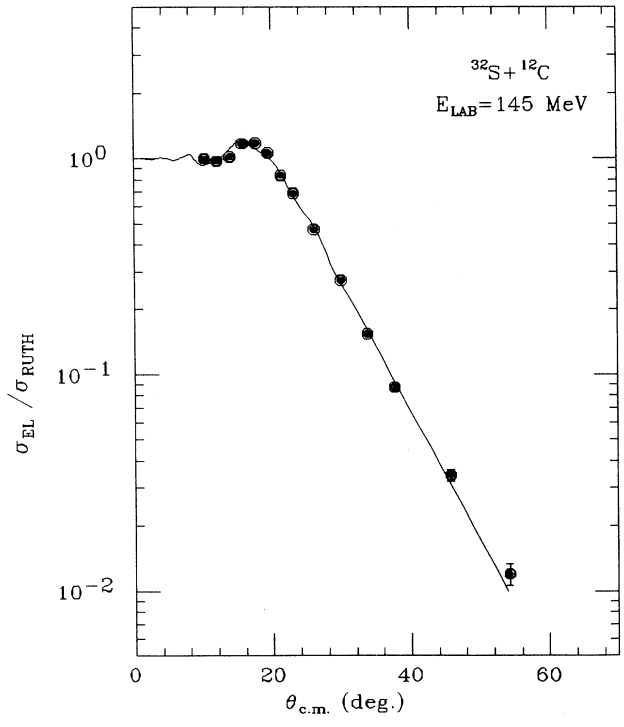

FIG. 4. Elastic-scattering cross section normalized to Rutherford scattering. The statistical errors are smaller than the data point size except where indicated. The solid line is the result of a fit to these data calculated by using PTOLEMY code.

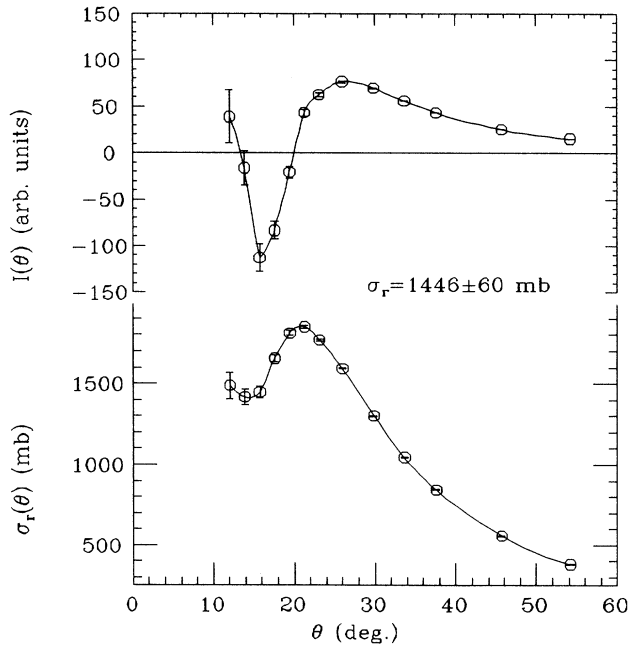

FIG. 5. The integrand function $I(\vartheta)$ (upper part) and the $\sigma_r(\vartheta)$ function (lower part) vs $\vartheta_{c.m.}$.

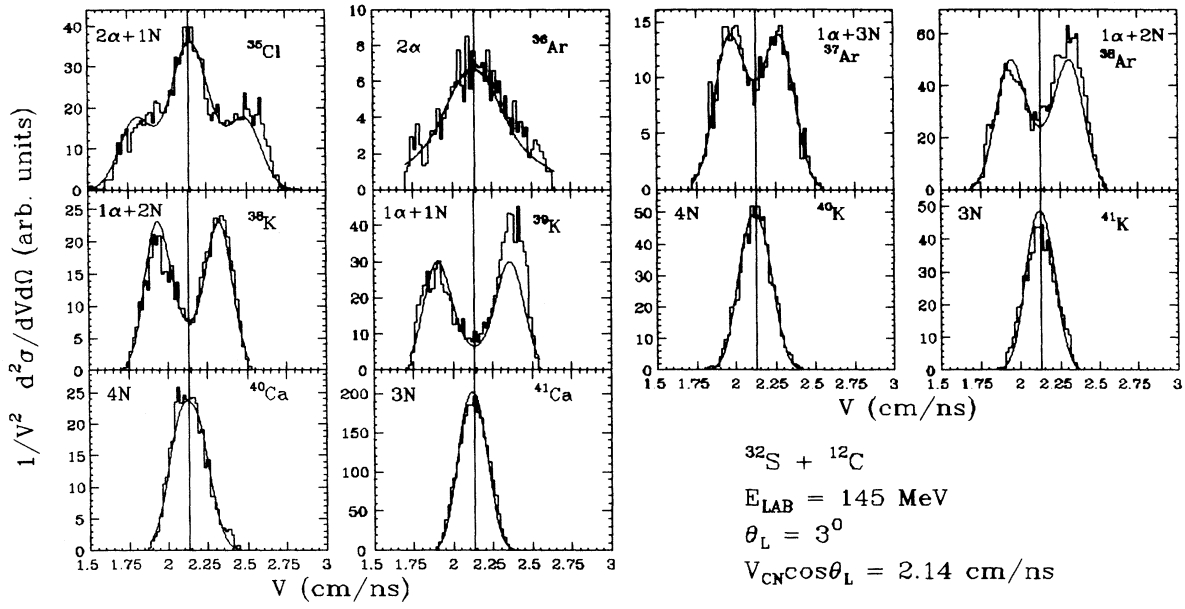

FIG. 6. Velocity spectra for evaporation residue masses $A_{ER}=35-41$ at $\vartheta_L=3°$. The histograms are the experimental data. The curves are calculated by means of formula (1) with the assumptions of Sec. IIIB. The vertical lines indicate the compound nucleus velocity $V_{CN}\cos\vartheta_L$. For each residue the numbers of evaporated α particles and nucleons (N) are indicated.

ly correct only for those residues ($A_{ER}=40$ and 41) resulting from nucleon evaporation. When this holds true, because no structure in the velocity distributions was observed other than symmetric Gaussian one, we concluded that these residues are reached purely by single (xp,yn) emission.

The presence of α-particle emission causes the appearance of structures. In fact the velocity spectrum of the residue shows a characteristic double peak corresponding to a single α-particle emission in the forward and backward directions. The centroids of these two peaks are shifted away from $\bar{V}_R=V_{CN}\cos\vartheta_L$ by the average recoil

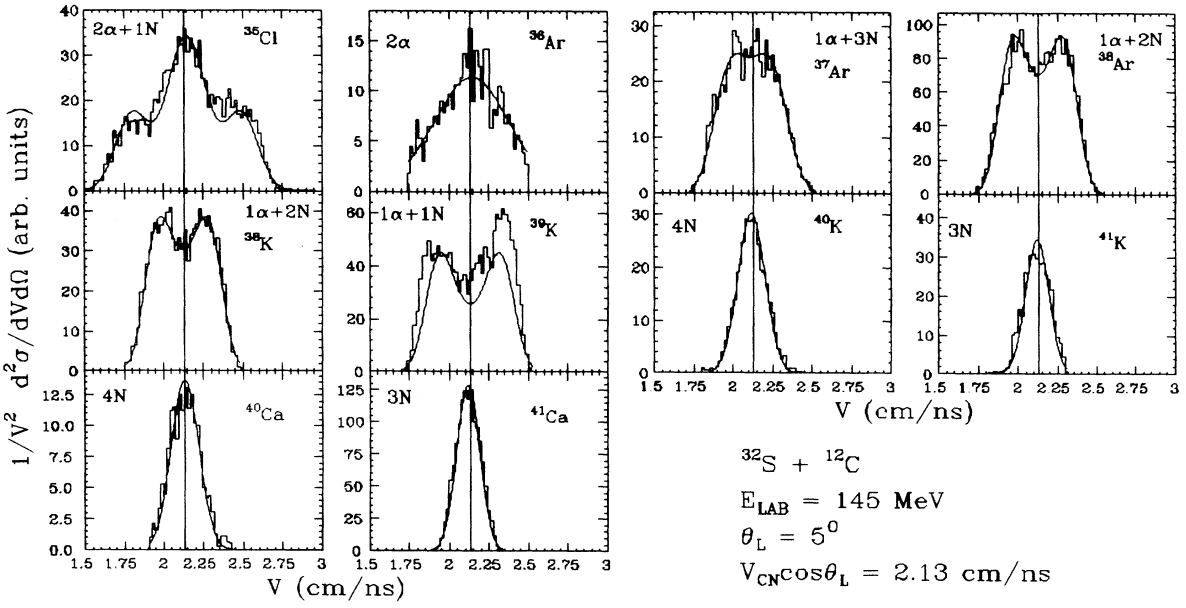

FIG. 7. Same as Fig. 6, but for $\vartheta_L=5°$.

velocity given to the residue by the emitted α particles.

The velocity spectra of the masses with $A_{ER}=37,38$ typically have this structure. To fit these velocity distributions we had to alter the exponent in Eq. (1). As pointed out previously in literature [21], to include evaporation of α particles we replaced the term $[(V_R - V_{CN}\cos\vartheta_L)^2 - V_{CN}^2\sin^2\vartheta_L]$ by $\{[(V_R - V_{CN}\cos\vartheta_L) + V_{CN}^2\sin^2\vartheta_L]^{1/2} - V_\alpha\}^2$. For ^{39}K we can see a small additional cross section at the high-energy peak which can be explained as coming from the ^{32}S(^{12}C,^{4}He)^{40}Ca* reaction with a following proton evaporation.

The velocity spectra of the $A=35$ mass show three peaks corresponding to the three possible combinations of the emission directions of the two α particles: forward-forward, forward-backward, and backward-backward. These spectra were well fitted considering a $2\alpha+1p$ emission.

In Fig. 8(a) and 8(b) the velocity distributions of ^{36}Ar at $\vartheta_L=3°$ and 5°, respectively, are reported. In addition to a broad symmetric peak centered at $\bar{V}_R=V_{CN}\cos\vartheta_L$ due to the evaporation of two α particles, both spectra show an high-energy peak, which can correspond to an ^{36}Ar coming from the ^{32}S(^{12}C,^{8}Be)^{36}Ar reaction. However, the clear separation of the two components allows us to easily subtract this contribution and to fit the remaining experimental data with a curve corresponding to the evaporation of two α particles, as is shown in Figs. 6 and 7, respectively.

Figure 9 shows for each evaporation residue, the ratios of the velocity centroids $V_{CN}\cos\vartheta_L$, expected in the case of complete fusion, to the $\bar{V}_R$ ones obtained by fitting the experimental velocity spectra. We can see that the ratio $V_{CN}\cos\vartheta_L/\bar{V}_R$ is equal to 1.0 for all the evaporation residues. The error bars include the statistics, the fitting process, and the energy-loss calculation uncertainties.

In Fig. 10 are reported the ratios of the full width at

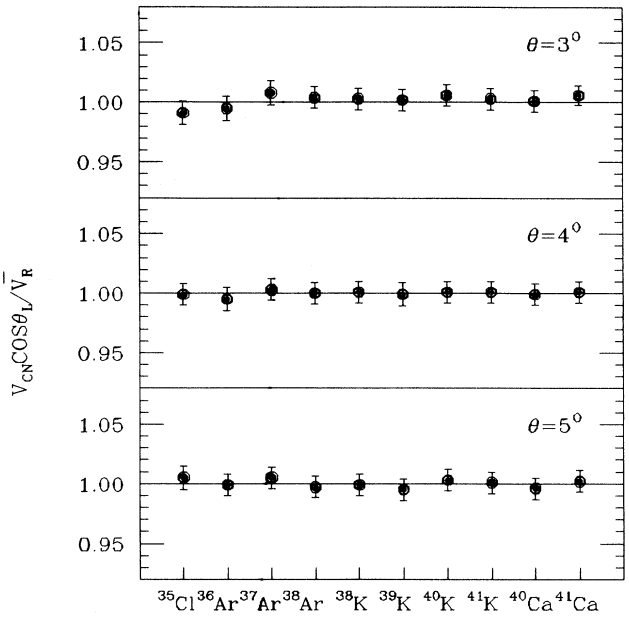

FIG. 9. Ratio of velocity centroids expected in the case of complete fusion to those obtained by fitting experimental velocity spectra plotted vs evaporation residues.

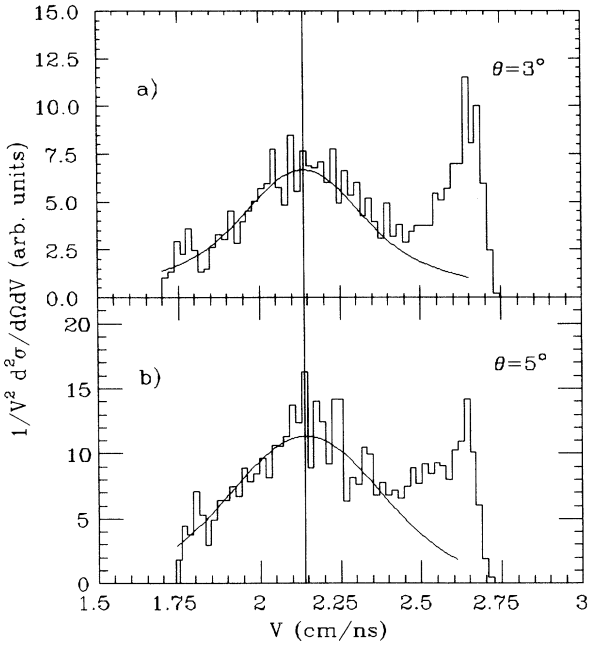

FIG. 8. Velocity distribution of ^{36}Ar detected at (a) $\vartheta_L=3°$ and (b) $\vartheta_L=5°$. The histograms are experimental distributions, while the solid lines are the fits obtained for the emission of two α particles.

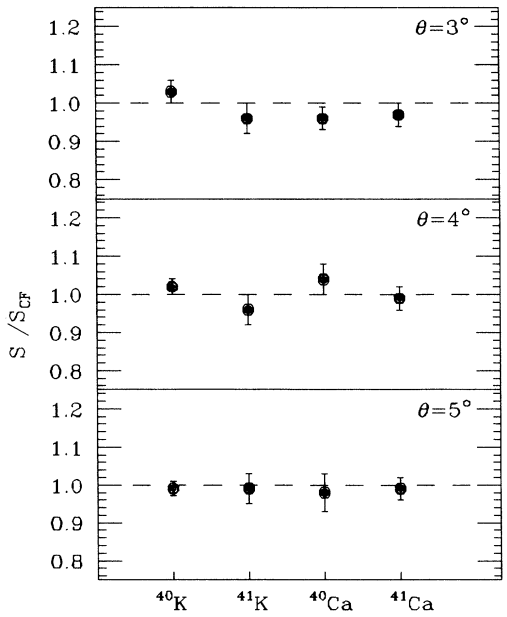

FIG. 10. Comparison of measured widths (FWHM) of individual product masses with the values expected in the case of complete fusion.

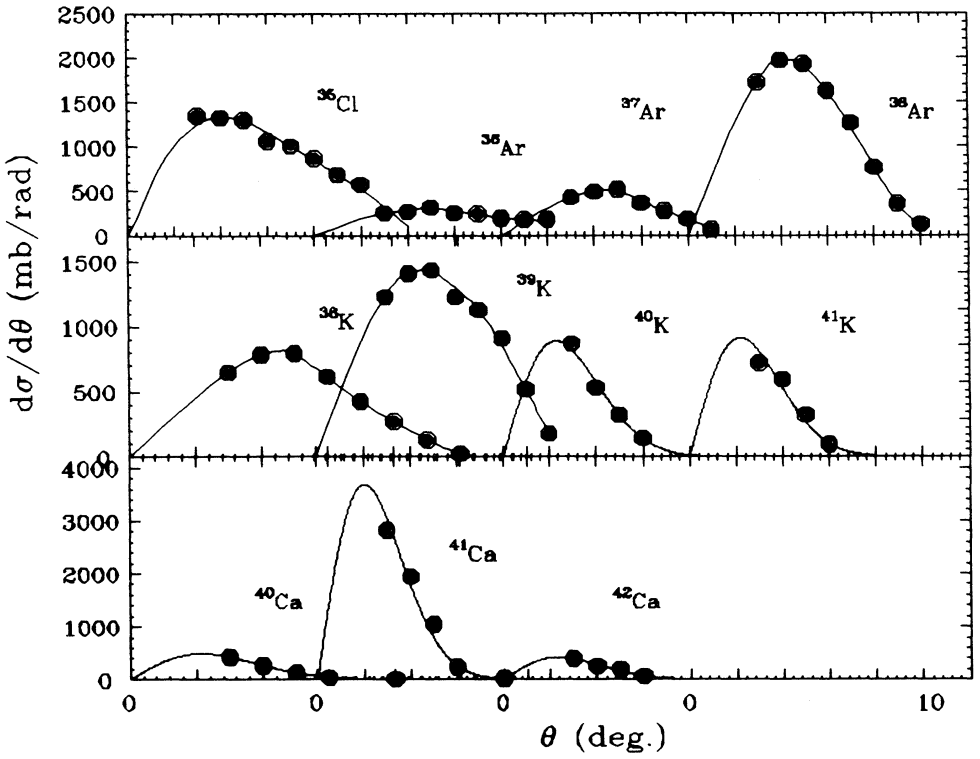

FIG. 11. Angular distributions of the evaporation residues. The lines are polynomial fits providing integrated cross sections.

half maximum (FWHM) of velocity distribution s, as obtained by fit to the one corresponding to a complete fusion s_{CF}. The latter has been calculated following Hilscher *et al.* [22] as $s^2_{CF}=n_{evap}T/(A_{ER})^2$. Here $n_{evap}=A_{CN}-A_{ER}$ is the number of evaporated nucleons and T is the compound nucleus temperature, as deduced from the formula $T=(8E_{exc}/A_{CN})^{1/2}$ in which the value $A_{CN}/8$ for the level density parameter is assumed.

Also in this case the value of the ratio is about 1.0 for all the considered masses. In conclusion, the inclusive velocity spectra of separated individual masses show a main contribution with typical structures due to nucleon (xp,yn) and α particle plus nucleon evaporation originating from evaporation residue following complete fusion. For some masses ($A=36$ and 39) an additional contribution which can be explained [23] as resulting from incomplete fusion reactions (^{12}C,^{8}Be) and (^{12}C,^{4}He) which correspond to a capture of ^{4}He and ^{8}Be, respectively, is observed.

TABLE II. Partial and total fusion cross sections measured for the evaporation residues detected in the present experiment.

$^{32}S+^{12}C$	$E_{LAB}=145$ MeV
^{35}Cl	195±19
^{36}Ar	46 ±5
^{37}Ar	48 ±5
^{38}Ar	201±20
^{38}K	76 ±8
^{39}K	142±14
^{40}K	54 ±5
^{41}K	62 ±6
^{40}Ca	27 ±3
^{41}Ca	229±23
^{42}Ca	32 ±3
Sc	11 ±1
$\sigma^{tot}_{fus}=1123\pm40$ mb	

C. Angular distributions

The experimental angular distribution $d\sigma/d\vartheta$ for complete fusion evaporation residues at the studied energy are shown in Fig. 11, and they were used to determine the fusion cross sections for each evaporation residue by means of polynomial fits.

The major source of error in the determination of these cross sections arises from the use of the elastic scattering to normalize the data.

As discussed earlier, indeed, the absolute cross-section scale setting was based on the requirement that the ratio of elastic to Rutherford scattering approaches unity at forward angles. Other small sources of error reflect the statistics of the experimental data and the uncertainty in the fits to the angular distributions, including the extrapolations to small and large angles. The fusion cross sections so obtained, with their estimated uncertainties are listed in Table II.

IV. COMPARISON WITH THEORY AND DISCUSSION

The experimental relative yields of the residue masses are shown in Fig. 12, together with the statistical model predictions computed using the LILITA [24] code. We remind the reader that the Monte Carlo Hauser-Feshbach LILITA code uses the sharp-cutoff approximation $\sigma_{\rm fus}=\pi\lambda^2(l_{\rm cr}+1)^2$ in the entrance channel. The compound nucleus is allowed to deexcite only by successive emission of protons, neutrons, α particles, and γ rays. The transmission coefficients of the exit channels are calculated by using a Fermi-function approximation.

$$T_{l_\alpha}(E_{\rm c.m.})=\frac{C_\alpha}{1+\exp[(B_{l_\alpha}-E_{\rm c.m.})/\Delta B_{l_\alpha}]}\ ,$$

where B_l is the sum of the Coulomb and centrifugal barriers, α denotes the particle type, and C_α and Δ are numerical parameters. The parametrization of the transmission coefficients is achieved by fitting the above function to the optical model T_l's.

The code uses two different approximations for the density of levels in the residual nucleus. For the low-excitation energy region a uniform level density as computed from known discrete levels is used. For high energies, LILITA calculates the level densities by using a constant temperature approximation of the Fermi-gas formula [25]. The pairing energies are given in Ref. [25] and the level density parameter a is taken equal to $A/7.5$. The spin-cutoff parameter is given by $2\sigma^2=2(J_{\rm rig}/\hbar^2)T$, where T is the nuclear temperature. $J_{\rm rig}$ is calculated with a $r_0=1.4$ fm radius parameter.

A satisfactory agreement between the experimental data and the LILITA calculations is found especially for residue masses neighboring the compound nucleus. Some discrepancies in the fine structure of the mass distributions may result from inadequacies of the transmission probabilities and of the level density modeling. The Monte Carlo LILITA code also permits the calculation of angular distributions of the evaporation residue. The results of these calculations reproduce very well the experimental angular distributions for evaporation residues with $Z=17$ up to 20, as shown in Fig. 13. The observed consistency of the experimental mass distributions and Z angular distributions with the statistical model calculations performed in the framework of the Hauser-Feshbach formalism confirms the previous conclusion that the main contribution to the residue cross section comes from complete fusion mechanism.

Figure 14 shows the experimental fusion and reaction cross sections available to date on the $^{32}S+^{12}C$ system as a function of $E_{\rm c.m.}^{-1}$. There, the closed symbols (circle for fusion and triangle for reaction cross section) are the present results, while the open symbols (circles and triangles at higher energy and squares at lower energies) are taken from Giordano *et al.*, [2] Arena *et al.*, [3], and Kolata *et al.* [1], respectively. These data are quoted with errors ranging between 6% and 10% as indicated by the authors.

At the highest measured energies a difference between reaction and fusion cross sections is observable. This can be interpreted as due, essentially to the contribution of direct processes as, for example, deep inelastic or transfer reactions.

In the same figure, the comparisons between the fusion cross sections and the predictions of the phenomenological formulas suggested by Lozano and Madurga [26] (dashed line), Kailas and Gupta [27] (dot-dashed line), and by some of us [28] (solid line) is shown. We recall that the formulas of Refs. [26,27] are based on a parametrization of the fusion cross section which involves an energy-dependent term for the fusion radius. These authors define the fusion cross section at the bombarding energy E (MeV) in the center-of-mass system for interacting nuclei (Z_1,A_1) and (Z_2,A_2) as $\sigma_{\rm fus}=\pi\rho(\rho-D)$, where $D=1.44(Z_1Z_2/E)$ is the minimum distance in a head-on collision between pointlike particles. They consider explicitly only the Coulomb potential, and

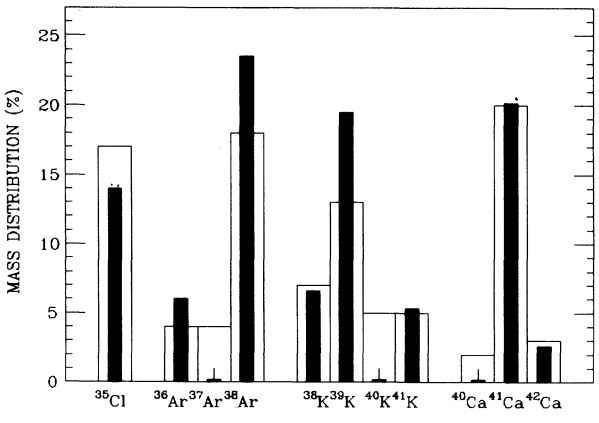

FIG. 12. Relative yields of evaporation residues. The data are plotted as open histograms, while the full bars are the relative yields predicted from evaporation code LILITA.

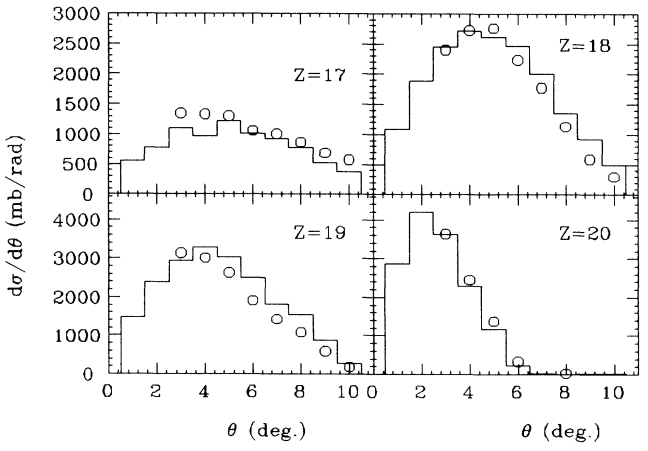

FIG. 13. Comparison of experimental angular distributions with the predictions of evaporation LILITA code (histograms) for each $Z>16$ detected.

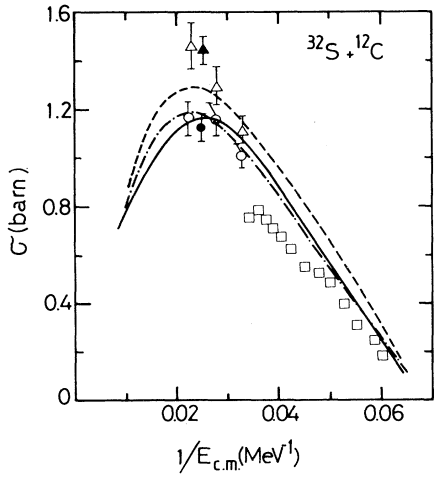

FIG. 14. Fusion and total reaction cross sections for the $^{32}S+^{12}C$ system as a function of $E_{c.m.}^{-1}$. Closed symbols are data of the present work; open symbols are taken from Refs. [1–3]. For an explanation of the curves see the text.

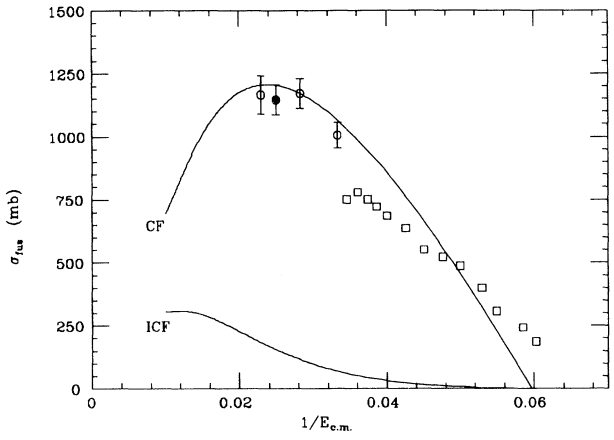

FIG. 15. Comparison of fusion experimental data with the prediction of the formula for complete fusion cross sections; the lower curve is the prediction of the incomplete fusion contribution for the system $^{32}S+^{12}C$.

$\rho = mE + b$ (with m and b parameters) is the generalized nuclear radius which depends on the energy in order to simulate the effects of nuclear interaction. The different procedures followed for fixing the m and b parameters distinguish the work of these authors.

As a consequence of the modified SOD method [18,19], the following empirical formula involving few parameters has been suggested for fusion cross sections [2].

$$\sigma_{\text{fus}} = \frac{C_1}{E} F(E) \left[C_2 F(E) - \frac{C_3}{\sqrt{E}} \right],$$

where

$$C_1 = \frac{\pi}{4.78} \frac{(A_1 + A_2)^2 (A_1^{1/3} + A_2^{1/3})}{A_1 A_2},$$

$$C_2 = (A_1 + A_2)(A_1^{1/3} + A_2^{1/3}),$$

$$C_3 = 0.316 Z_1 Z_2 \left[\frac{A_1 A_2}{A_1 + A_2} \right]^{1/2},$$

and

$$F(E) = a_0 (1 - \Delta^n) \left[1 - \exp\left[-b \frac{E}{A_1 + A_2} \right] \right].$$

Here $\Delta = (A_1 - A_2)/(A_1 + A_2)$ is the asymmetry parameter and A_1, A_2, Z_1, Z_2 are the mass and the charge numbers of the colliding nuclei, respectively, E is the center-of-mass energy in MeV, and σ_{fus} is expressed in barns. The values of n, a_0, and b are fixed following the prescriptions of the Ref. [2].

By looking at Fig. 14, we can make some remarks on these comparisons. The calculation of Lozano and Madurga overestimates the experimental fusion cross section in the whole considered energy range. The formula of Kalais and Gupta is in fairly good agreement with experimental data in the second energy region, but the predicted maximum seems to be slightly shifted with respect to the experimental one. In the low-energy region also, this calculation overestimates the experimental fusion cross section.

The curve derived from the modified SOD method is in quite good agreement with the experimental data in the intermediate energy region and reproduces in a very satisfactory way the value of the maximum and the energy at which it occurs. However, also in this case the experimental points at low energy are not well fitted.

Finally, in Fig. 15 the fusion experimental data and the predictions of a formula, recently proposed for complete fusion cross sections [29], are reported. This formula is derived in the framework of the "elastic model" [30] by assuming that the "effective potential" attains a maximum value (or a horizontal inflection point) and that r_f, the relative distance of the colliding systems, can be expressed as a linear function of $E/(A_1 + A_2)$, where E is the center-of-mass energy and A_1, A_2 are the mass numbers. This linear dependence of r_f on the energy allows us to express the fusion cross section $\sigma_f(E)$ as a simple function of the energy. However, in order to determine $\sigma_f(E)$ it is necessary to know the value of $\sigma_f(E_1)$ at an arbitrary value E_1 of the energy.

According to this model the complete fusion cross section can be calculated by means of the formula

$$\sigma_{\text{CF}}(E) = \left[a_1 E^2 - a_2 E + a_3 + \frac{b_1}{E} \right] \times \left\{ 1 - \exp\left[-2.789 \left[\frac{E_m}{E} \right]^{\beta} \right] \right\}. \quad (2)$$

where

$$a_1 = \frac{\pi \alpha^2}{3(A_1 + A_2)^2}, \quad a_2 = \frac{\pi \alpha r_1}{A_1 + A_2}, \quad a_3 = \pi r_1^2,$$

with

$$\alpha = 6.00 \text{ fm/MeV} ,$$

$$r_1 = r_0 \left[1 - \exp\left[- \frac{(A_1 + A_2)^{2/3}}{10} \right] \right] ,$$

$$r_0 = 16.75 \left[1 - \exp\left[- \frac{1}{\chi^2} \right] \right] \text{ fm}, \quad \chi = \left| \frac{A_1 - A_2}{A_1 + A_2} \right| .$$

$$b_1 = E_1 \sigma_f(E_1) - a_3 E_1 + a_2 E_1^2 - a_1 E_1^3 ,$$

and β, a dimensionless parameter, is equal to 5.5.

Under the assumption that the incomplete fusion process occurs at all bombarding energies with no apparent energy threshold, in Ref. [29] the following phenomenological formula has been suggested:

$$\sigma_{\text{ICF}} = \sigma_{\text{CF}} \exp\left[- \frac{E_M}{E} (2.86 - 2\chi) \right] , \tag{3}$$

where σ_{CF} is defined by Eq. (2) and E_M is the value of the energy at which the fusion cross section attains its maximum.

By an inspection of the Fig. 15, we note that there is satisfactory agreement between the experimental data and the prediction of formula (2), especially in the intermediate energy region. In the same figure the predictions of formula (3) for the incomplete fusion cross section are also reported. At the energy at which we carried out our experiment, the predicted value of the incomplete fusion cross section is about 13% of σ_{CF}. This prediction disagrees with the small incomplete fusion contributions in the evaporation residue cross section found in our kinematic analysis.

V. SUMMARY AND CONCLUSIONS

In this paper we have presented the elastic-scattering cross section and the mass and angular distributions for the evaporation residues produced in the reaction $^{32}S + ^{12}C$ at a bombarding energy of 4.5 MeV/nucleon. The total reaction cross section obtained by using the modified SOD method is in excellent agreement with the value obtained by means of the optical model analysis.

From the kinematical analysis of the inclusive velocity spectra we can deduce that the main contribution of the evaporation residue cross section originates from complete fusion mechanisms, but also at this low bombarding energy, there is evidence for incomplete fusion processes coming from the (^{12}C,^{4}He) and (^{12}C,^{8}Be) reactions. The experimental Z angular distributions ($d\sigma/d\vartheta$), and the mass distribution are in good agreement with the predictions of the LILITA evaporation code.

Finally, the fusion excitation functions calculated by means of phenomenological formulas show a satisfactory agreement with the available experimental data, especially in the intermediate energy region, while the predictions of an analytical expression recently suggested to account for the incomplete fusion contributions overestimates them and disagrees with present experimental results.

ACKNOWLEDGMENTS

The authors wish to thank the Laboratorio Nazionale del Sud (Catania) accelerator staff for their assistance in providing the beam used in our experiment. Thanks are due to V. Campagna and G. Poli for their technical help during the measurements, as well as to Dr. A. Anzalone and Dr. F. Giustolisi for their kind cooperation in preparing the data acquisition software. The authors would like also to thank Professor G. La Rana for making available the LILITA code and for helping with computer calculations.

[1] J. J. Kolata, R. A. Racca, P. A. De Young, E. Aguilera-Reyes, and M. A. Xepses, Phys. Rev. C **32**, 1080 (1985).
[2] R. Giordano, F. Porto, S. Sambataro, and A. Scalia, Nuovo Cimento A **77**, 135 (1983).
[3] N. Arena, Seb. Cavallaro, S. Sambataro, S. Femino', F. Porto, A. Anzalone, and P. Figuera, Nuovo Cimento A **100**, 953 (1988).
[4] O. R. Zolnowski, H. Yemeda, S. E. Cola, A. C. Kehler, and T. T. Sugihara, Phys. Rev. Lett. **41**, 92 (1978).
[5] T. Udagawa and T. Tamura, Phys. Lett. **116B**, 311 (1982).
[6] K. Siwek-Wilczynski, E. H. du Merclue Van Voorthnyser, J. Van Pepta, R. H. Siemssen, and J. Wilczynski, Phys. Rev. Lett. **42**, 1599 (1979); Nucl. Phys. **A330**, 150 (1979).
[7] H. Morgenstern, W. Bohne, W. Golster, K. Grabisch, and A. Kyenowski, Phys. Rev. Lett. **52**, 1104 (1984).
[8] G. S. Stephen, D. G. Kevar, R. V. F. Jeusseus, G. Rosner, H. Ikezoe, B. Wilkins, D. Hendusan, K. T. Lesko, J. J. Kolata, C. K. Gelbke, B. V. Jacak, Z. M. Koenig, G. D. Westfall, A. Szanto de Toledo, E. M. Szanto, and P. L. Gonthier, Phys. Lett. **161B**, 60 (1985).
[9] D. G. Kovar, in *Proceedings of the 5th Adriatic International Conference on Nuclear Physics, Croatia, Yugoslavia, 1984,* edited by N. Cindro, W. Greiner, and R. Caplar (World Scientific, Singapore, 1984), pp. 185–204.
[10] J. P. Coffin, in *Proceedings of the 6th Adriatic International Conference on Nuclear Physics, Dubrovnik, Yugoslavia, 1987,* edited by N. Cindro, W. Greiner and R. Caplan (World Scientific, Singapore, 1987), p. 227, and references cited therein.
[11] G. S. F. Stephans *et al.*, Phys. Lett. **161B**, 60 (1985).
[12] D. J. Parker *et al.*, Phys. Rev. C **35**, 167 (1987).
[13] I. Tserruya, V. Steiner, Z. Fraenkal, P. Jacoles, D. G. Kovar, W. Henning, M. F. Vineyard, and B. G. Glagola, Phys. Rev. Lett. **60**, 14 (1988).
[14] F. Porto, S. Sambataro, and F. Santonocito, Laboratorio Nazionale del Sud Report No. 87/1, 1987.
[15] P. Figuera, F. Porto, S. Sambataro, and G. Poll, Laboratorio Nazionle del Sud Report No. 87/2, 1987.

[16] P. Figuera, S. Pirrone, A. Anzalone, N. Arena, Seb. Cavallaro, S. Femino', F. Giustolisi, F. Porto, and S. Sambataro, Nuovo Cimento A **104**, 251 (1991).
[17] M. H. Farlane and S. C. Poeper, Argonne National Laboratory Report No. ANL-76-11, 1978.
[18] R. Giordano, F. Porto, S. Sambataro, and A. Scalia, Nuovo Cimento A **61**, 182 (1981).
[19] R. Giordano, F. Porto, S. Sambataro, and A. Scalia, Nuovo Cimento **31**, 189 (1981).
[20] J. Gomez del Campo, R. G. Stokstad, J. A. Biggerstoff, R. A. Dayras, A. H. Snell, and P. H. Stelson, Phys. Rev. C **19**, 2170 (1979).
[21] H. Morgernsten, W. Bohne, W. Grabish, H. Lehr, and W. Stoffler, Z. Phys. A **313**, 39 (1983).
[22] D. Hilscher, J. R. Birkelund, A. D. Hoover, W. U. Schnoder, W. W. Wilcke, J. R. Huizenga, A. C. Mignerey, K. L. Wolf, H. F. Brener, and V. E. Viola, Jr., Phys. Rev. C **20**, 576 (1979).
[23] H. Morgenstern, W. Bohne, W. Galster, and K. Grabisch, Z. Phys. A **324**, 443 (1986).
[24] J. Gomez del Campo and R. G. Stokstad, "LILITA, a Monte Carlo Statistical Model Code," Oak Ridge National Laboratory Technical Memo No. ORNL-TM-7295, 1981 (unpublished).
[25] A. Gilbert and A. G. W. Cameron, Can. J. Phys. **43**, 1446 (1965).
[26] M. Lozano and G. Madurga, Phys. Lett. **90B**, 50 (1980).
[27] S. Kailas and S. K. Gupta, Z. Phys. A **302**, 355 (1981).
[28] F. Porto and S. Sambataro, Nuovo Cimento A **83**, 329 (1984).
[29] A. Scalia, R. Giordano, S. Sambataro, F. Porto, P. Figuera, and S. Pirrone, Nuovo Cimento A **103**, 269 (1990).
[30] A. Scalia, Nuovo Cimento A **88**, 437 (1985).